Paleoceanography and Paleoclimatology

RESEARCH ARTICLE
10.1029/2019PA003842

Special Section:
The Miocene: The Future of the Past

Simulated Thermohaline Fingerprints in Response to Different Greenland-Scotland Ridge and Fram Strait Subsidence Histories

Akil Hossain[1], **Gregor Knorr**[1], **Gerrit Lohmann**[1], **Michael Stärz**[1], **and Wilfried Jokat**[1]

[1]Alfred Wegener Institute, Helmholtz-Centre for Marine and Polar Research, Bremerhaven, Germany

Abstract Changes in ocean gateway configuration can induce basin-scale rearrangements in ocean current characteristics. However, there is large uncertainty in the relative timing of the Oligocene/Miocene subsidence histories of the Greenland-Scotland Ridge (GSR) and the Fram Strait (FS). By using a climate model, we investigate the temperature and salinity changes in response to the subsidence of these two key ocean gateways during early to middle Miocene. For a singular subsidence of the GSR, we detect warming and a salinity increase in the Nordic Seas and the Arctic Ocean. As convection sites shift to the north of Iceland, North Atlantic Deep Water (NADW) is formed at cooler temperatures. The associated deep ocean cooling and upwelling of deep waters to the Southern Ocean surface can cause a cooling in the southern high latitudes. These characteristic responses to the GSR deepening are independent of the FS being shallow or deep. An isolated subsidence of the FS gateway for a deep GSR shows less pronounced warming and salinity increase in the Nordic Seas. Arctic temperatures remain unaltered, but a stronger salinity increase is detected, which further increases the density of NADW. The increase in salinity enhances the contribution of NADW to the abyssal ocean at the expense of the colder southern source water component. These relative changes largely counteract each other and cause a negligible warming in the upwelling regions of the Southern Ocean.

Key Points:
- Deepening of the Greenland-Scotland Ridge (GSR) causes warming and a salinity increase in the Nordic Seas and Arctic Ocean
- The characteristic temperature and salinity changes are independent of the Fram Strait gateway configuration
- Fram Strait subsidence for a deep GSR causes less pronounced warming and salinity increase in the Nordic Seas

Supporting Information:
- Supporting Information S1

Correspondence to:
A. Hossain,
akil.hossain@awi.de

Citation:
Hossain, A., Knorr, G., Lohmann, G., Stärz, M., & Jokat, W. (2020). Simulated thermohaline fingerprints in response to different Greenland-Scotland Ridge and Fram Strait subsidence histories. *Paleoceanography and Paleoclimatology*, *35*, e2019PA003842. https://doi.org/10.1029/2019PA003842

Received 19 DEC 2019
Accepted 25 APR 2020
Accepted article online 13 MAY 2020

Author Contributions:
Conceptualization: Akil Hossain, Gregor Knorr, Gerrit Lohmann, Wilfried Jokat
Formal analysis: Akil Hossain, Gregor Knorr
Funding acquisition: Gerrit Lohmann, Wilfried Jokat
Investigation: Akil Hossain, Gregor Knorr
(continued)

1. Introduction

Changes in ocean gateway geometry play a key role in global climate evolution throughout the Cenozoic (65 Myr ago to present) (Bartoli et al., 2005; Elsworth et al., 2017; Haug & Tiedemann, 1998; Stärz et al., 2017). Deep-water formation in the northern high latitudes is a key driver of the global ocean circulation as well as global climate (Aagaard & Carmack, 1994; Jakobsson et al., 2007). The formation of Atlantic-Arctic gateways (i.e., Fram Strait [FS], Greenland-Scotland Ridge [GSR]) drives northward-directed oceanic heat transport (Stärz et al., 2017). The geometrical widening/subsidence of the northern gateway configuration drove water mass and large-scale circulation changes (Jakobsson et al., 2007; Wright & Miller, 1996). In this context, a threshold in ocean gateway depth, that is linked to the effect of wind mixing (Stärz et al., 2017), is an important parameter. Intensive glaciations at the Earth's polar region during the Cenozoic have been linked to the opening of the ocean gateways (Knies & Gaina, 2008). Geological data indicate that the Barents Sea region is subaerially exposed during most of the Cenozoic (Butt et al., 2002; Hutchinson et al., 2019). In the critical time period during Oligocene/Miocene transition, FS was the only deep-water connection of the Arctic with the World Oceans (Ehlers & Jokat, 2013; von Appen et al., 2015). Consequently, the continuous opening of the FS played a crucial role in ocean dynamics of the Arctic Ocean and therefore in the evolution of the northern polar region (Ehlers & Jokat, 2013; Jakobsson et al., 2007; Jokat et al., 2016). This also likely caused an intensification of the North Atlantic thermohaline circulation (Knies et al., 2014). The ventilation of the Arctic Ocean was established with the opening of FS to a critical width (about 40–50 km) that allowed entrance of saline Atlantic waters to the Arctic and supplied oxygen to intermediate/deep waters (Jakobsson et al., 2007). However, further south of the FS, the GSR constitutes an ocean gateway between the Atlantic Ocean and the Nordic Seas (located between FS and GSR) (Davies et al., 2001; Stärz et al., 2017; Thiede & Myhre, 1996; Via & Thomas, 2006; Wright & Miller, 1996). The subsidence of the GSR sill depth deeper than the wind mixed layer (~50 m) strengthens the entrainment of Atlantic waters, and a bidirectional circulation across the ridge develops, creating a baseline for the final establishment of a modern prototype current system (Stärz et al., 2017). The formation of North Atlantic Deep Water (NADW) releases heat

Methodology: Akil Hossain, Michael Stärz
Supervision: Gerrit Lohmann, Wilfried Jokat
Writing - original draft: Akil Hossain, Gregor Knorr
Writing – review & editing: Gregor Knorr, Gerrit Lohmann, Wilfried Jokat

to the atmosphere in the northern high latitudes (Broecker & Denton, 1989; Wright & Miller, 1996), and the progressive subsidence of GSR during the Miocene allowed increased export of NADW to the abyssal ocean (Knies et al., 2014; Poore et al., 2006). Transformation of these water masses associated with mixing and upwelling to the Southern Ocean surface is a key source of heat for summer sea ice melting around Antarctica (Gordon, 1981; Wright & Miller, 1996). Hence, changes in the relative timing of the North Atlantic gateway configuration not only are a key control for North Atlantic and Arctic environmental conditions but also bear the potential to have far field bi-polar impacts.

As yet, the relative timing of the subsidence of gateways between the Arctic Ocean and the northern North Atlantic, providing deep-water exchange and ventilation of the Arctic Ocean, has been poorly constrained by scientific drilling. Only few data exist to describe the subsidence of the GSR in great detail. Before initial GSR subsidence (~36 Ma), lagoonal circulation in the Nordic Seas restricted export of polar freshwater toward the Atlantic (DSDP Site 336; Talwani et al., 1976). Subsequently, drill samples indicate a progressive deepening of GSR around 36–31 Ma, which creates a semienclosed estuarine gateway exchange and brackish saline Nordic Seas. Around 20–24 Ma, the GSR sill is well below sea level and the wind-induced mixed layer establishing northward-directed warm North Atlantic Current flowing to the east of Nordic Seas and a southward cold East Greenland Current to the west (Stärz et al., 2017). The large knowledge gaps on the GSR subsidence, which formed by excess magma production of the Iceland plume, can only be filled by additional scientific drilling along the ridge. Standard subsidence models typical for oceanic crust cannot be applied. Plume pulsations, which might have caused a temporary uplift and/or slowed down the GSR subsidence, cannot be excluded. The situation in the FS is different. It formed by seafloor spreading between Greenland and Svalbard. A paleobathymetric model shows that the first possibility for a deep-water exchange between the North Atlantic and the Nordic Seas through GSR could have been between 15 and 20 Ma (Ehlers & Jokat, 2013). The timing for the emplacement of oceanic crust in the FS is much better constrained by geophysical data. Extensive seismic and magnetic data indicate that the FS was likely a shallow and narrow gateway close to 21 Ma (Jokat et al., 2016). Further, scientific drilling in the central Arctic indicate that the evolution of a poorly ventilated and landlocked sea to a ventilated Arctic Ocean initiated latest at ~18 Ma (Ehlers & Jokat, 2013; Jakobsson et al., 2007). Since then, the exchange of cold Arctic water and warm Atlantic water has been possible (Jakobsson et al., 2007). However, it remains a challenge to better constrain the relative timing of both northern gateways in order to understand their potential climatic responses.

Here, we investigate several different cases for the relative subsidence of both the GSR and the FS. In our numerical experiments, we use a fully coupled atmosphere-ocean-sea ice model to explore singular and combined effects of both gateways on ocean circulation and climate during a time interval between ~35 and 15 Ma. In our sensitivity studies, we apply Miocene (~23–15 Ma) background climate conditions (Stärz et al., 2017) as a basis and use different GSR and FS sill depths representing different possible tectonic configurations during the early to middle Miocene. Based on tectonic constraints, we interpret which scenarios are the most likely ones to provide fingerprints of characteristic thermohaline changes.

2. Materials and Methods

We apply the fully coupled Earth System Model COSMOS, which includes the atmosphere model ECHAM5 (Roeckner et al., 2003), the land-vegetation model JSBACH (Raddatz et al., 2007), and the ocean model MPI-OM (Marsland et al., 2003). The atmosphere model is used at T31 spherical horizontal resolution (~3.75° × 3.75°) with 19 vertical layers. The land-vegetation model runs at the same horizontal resolution as the atmosphere model. The ocean model is resolved at 40 uneven vertical layers and has a resolution of GR30 (3° × 1.8°). Close to the grid poles (e.g., Labrador and Nordic Seas), the spatial resolution is relatively high. The model dynamics are solved on a curvilinear Arakawa C-grid. The MPI-OM includes a Hibler-type dynamic-thermodynamic sea ice model. The interactive exchange of fluxes of energy, momentum, and mass between ocean and atmosphere is performed via the coupler OASIS3 (Jungclaus et al., 2006). The climate model has already been applied for scientific questions focusing on the last millennium (Jungclaus et al., 2010), the Holocene (Lohmann et al., 2013; Stärz et al., 2016; Wei & Lohmann, 2012), the Last Glacial Maximum (Gong et al., 2013; Stärz et al., 2016; Zhang et al., 2013), the Pliocene (Stepanek & Lohmann, 2012), and the Miocene (Huang et al., 2017; Knorr et al., 2011; Knorr & Lohmann, 2014; Stärz et al., 2017; Stein et al., 2016).

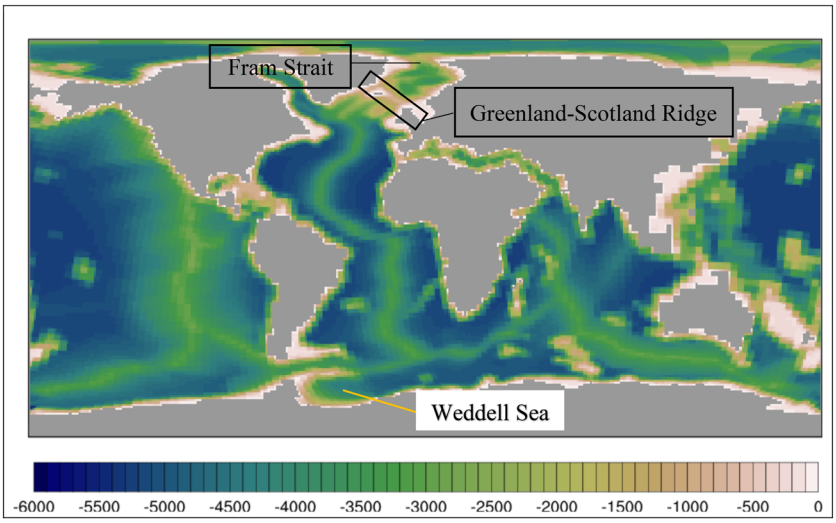

Figure 1. Global topography/bathymetry reconstruction (in m) (Herold et al., 2008) which is improved by high-resolution bathymetry reconstructions comprising the Arctic/North Atlantic sector for 15 Ma (Ehlers & Jokat, 2013) and the Weddell Sea embayment for 15 Ma (Huang et al., 2014).

The model setup is based on early to middle Miocene time period (~23–15 Ma) including orography, paleobathymetry, and ice sheet adjustments of Herold et al. (2008). Additionally, a regional high-resolution bathymetric reconstruction comprising the North Atlantic/Arctic Ocean (Ehlers & Jokat, 2013) is implemented in our approach. The original model setup of Stärz et al. (2017) is further refined by including a more realistic regional Weddell Sea bathymetry reconstruction in the Southern Ocean (Huang et al., 2017) (Figure 1). The ocean grid cells representing the Barents Sea region have been transferred to land cells. This assumption is in better agreement with geological data (Butt et al., 2002). Therefore, the FS represents a single gateway control toward the Arctic Ocean. Other ocean gateways like the Barents Sea, Canadian Archipelago, and Bering Strait evolved after the middle Miocene. Furthermore, the Panama Seaway and Tethys still connect the ocean basins. In general, the elevation of the Antarctic ice-sheet and the Miocene orography (Rocky Mountains, Tibetan Plateau, Andes, East Africa) are reduced compared to preindustrial (PI) times, whereas the Greenland ice-sheet is absent in our Miocene setup.

In our reference simulation (MIO_450), we prescribe an atmospheric CO_2 level of 450 ppm, and both gateways are fully developed (GSR depth: ~960 m; width: ~1,300 km and FS depth: ~2,500 m; width: ~500 km, Table 1). The ocean gateways are wide enough to maintain rotationally controlled exchange flows across the gateways (Pratt & Spall, 2008). We integrate the model for 4 kyr to minimize temperature/salinity trends in the deep ocean (Figures S17 to S20 in the supporting information) after initialization of the ocean from present day conditions (Figures S14 and S15). Based on this experiment, the ocean gateway sensitivity experiments are performed at various height dimensions of the GSR and FS. A list of our key model experiments including relevant model characteristics is summarized in Table 1. After model integration of at least 2 kyr, a climatological period of the final 100 yr of model simulation is used for analysis.

Table 1
List of Key Sensitivity Experiments Which Serve as a Basis for Key Scenarios (Listed in Table 2)

Model Exp.	Fram width (km)	Fram depth (m)	GSR depth (m)	Atmos. CO_2 (ppm)	Length of simulation (kyrs)
MIO_450	~500	~2,500	~960	450	3.3
MIO_FS50	~500	50	~960	450	2.0
MIO_GSR40	~500	~2,500	40	450	2.0
MIO_FS50_ GSR40	~500	50	40	450	2.0
PI	~670	~2,800	~1,100	280	5.9

Note. A set of 14 additional sensitivity experiments performed to collaborate our result are listed in Table S1.

Table 2
List of Key Scenarios

Title	Anomaly of experiments	GSR depth change (m)	FS depth change (m)
$\Delta GSR\_FS_{shallow}$	MIO_FS50 – MIO_FS50_GSR40	~960–40	50
ΔGSR_FS_{deep}	MIO_450 – MIO_GSR40	~960–40	~2,500
$\Delta FS\_GSR_{shallow}$	MIO_GSR40 – MIO_FS50_GSR40	40	~2,500–50
ΔFS_GSR_{deep}	MIO_450 – MIO_FS50	~960	~2,500–50
ΔGSR_ΔFS	MIO_450 – MIO_FS50_ GSR40	~960–40	~2,500–50

A previous study by Stärz et al. (2017) investigated the singular effect of GSR subsidence for a deep (~2,500 m depth) and wide (~500 km) FS. They found a nonlinear impact of sill depth on the Arctic Ocean circulation and water mass exchange that is mainly driven by the effect of gateway depth on mixed layer characteristics. In our study, we apply different GSR and FS states as a representative for different tectonic settings that occur during the subsidence interval to explore singular/combined effects of both gateways on ocean circulation and climate ~35 and 15 Ma. For this study, a shallow GSR means that it was subaerial or close to the surface (<40 mbsl) for its entire length.

In comparison to PI, a stronger surface circulation is driven by more direct wind forcing due to a nonpermanent (seasonal) sea ice cover and stronger stratification (baroclinic-geostrophic forcing) in the Arctic Ocean. From a Northern Hemisphere perspective, these characteristics in MIO_450 are similar to the modeled Miocene changes in Stärz et al. (2017), although the Barents Sea region is subaerially exposed in our setup. However, based on the implementation of an improved Weddell Sea bathymetry (Huang et al., 2014), there are fundamental changes in Antarctic bottom water (AABW) formation. In particular, the southerly placed shelf break in the Weddell Sea causes an increase of AABW formation and enhanced gyre transport in the Southern Ocean in accordance with Huang et al. (2017).

Using a set of four key model simulations (Table 1), we examine the isolated impacts of the GSR and FS subsidence by changing the sill depth, starting from a shallow depth toward a deep Miocene bathymetric configuration. The different model scenarios are specified in Table 2, and the analysis is supported by 14 additional sensitivity experiments (Table S1). In $\Delta GSR\_FS_{shallow}$, we consider a subsidence of GSR gateway depth from 40 to ~960 mbsl when FS sill depth is shallow (50 mbsl), and in scenario ΔGSR_FS_{deep}, the GSR is deepened to ~960 mbsl for a deep FS sill (~2,500 mbsl) to analyze the singular effect of GSR gateway subsidence. On the other hand, both model scenarios $\Delta FS\_GSR_{shallow}$ and ΔFS_GSR_{deep} are characterized by subsidence of FS from 50 to ~2,500 mbsl for a shallow (40 mbsl)/deep (~960 mbsl) GSR sill to investigate the singular effect of FS gateway deepening. In an additional model scenario (ΔFS_ΔGSR), the FS is deepened from 50 to ~2,500 mbsl in parallel with the GSR that is deepened from 40 to ~960 mbsl in order to test potential interaction and feedbacks between both gateways. To analyze the climate responses due to the relative timing of the subsidence histories of both ocean gateways, we primarily focus on the temperature/salinity changes.

3. Results

3.1. Singular Effect of GSR Deepening for a Shallow FS ($\Delta GSR\_FS_{shallow}$)

A singular subsidence of GSR from 40 mbsl toward a deep gateway configuration of ~960 mbsl for a shallow FS ($\Delta GSR\_FS_{shallow}$) enhances the entrance of Atlantic waters to the Nordic Seas (Figures 2a and 2b). In parallel with GSR subsidence, the corresponding salt water exchange across the gateway largely controls the overall salinity increase at the ocean surface in both the Nordic Seas and the Arctic Ocean (Figure 3b). We observe a cooling and unchanged salinity conditions south of Iceland. As more cold water from the polar and subpolar Arctic is advected southward, the overflow and the deep water south of Iceland becomes cooler (up to −2 K).

In the Nordic Seas, a warming (up to +7 K) in combination with reduced sea ice cover and a salinity increase (up to +14 psu) is simulated as the GSR subsides. In the Arctic Ocean, a salinity increase (up to +4 psu) (Figure 3) and warming in subsurface water (between 100 and 1,000 m; up to +2 K) linked with reduced sea ice extent is detected (Figures 4 and 5). The convection sites shift to the north off Iceland. Therefore, deep water formation takes place at cooler temperatures. Across the GSR, relatively saline and warm water is transported north-eastwards in the near-surface/subsurface layers (upper ~500 m), while cold but fresher

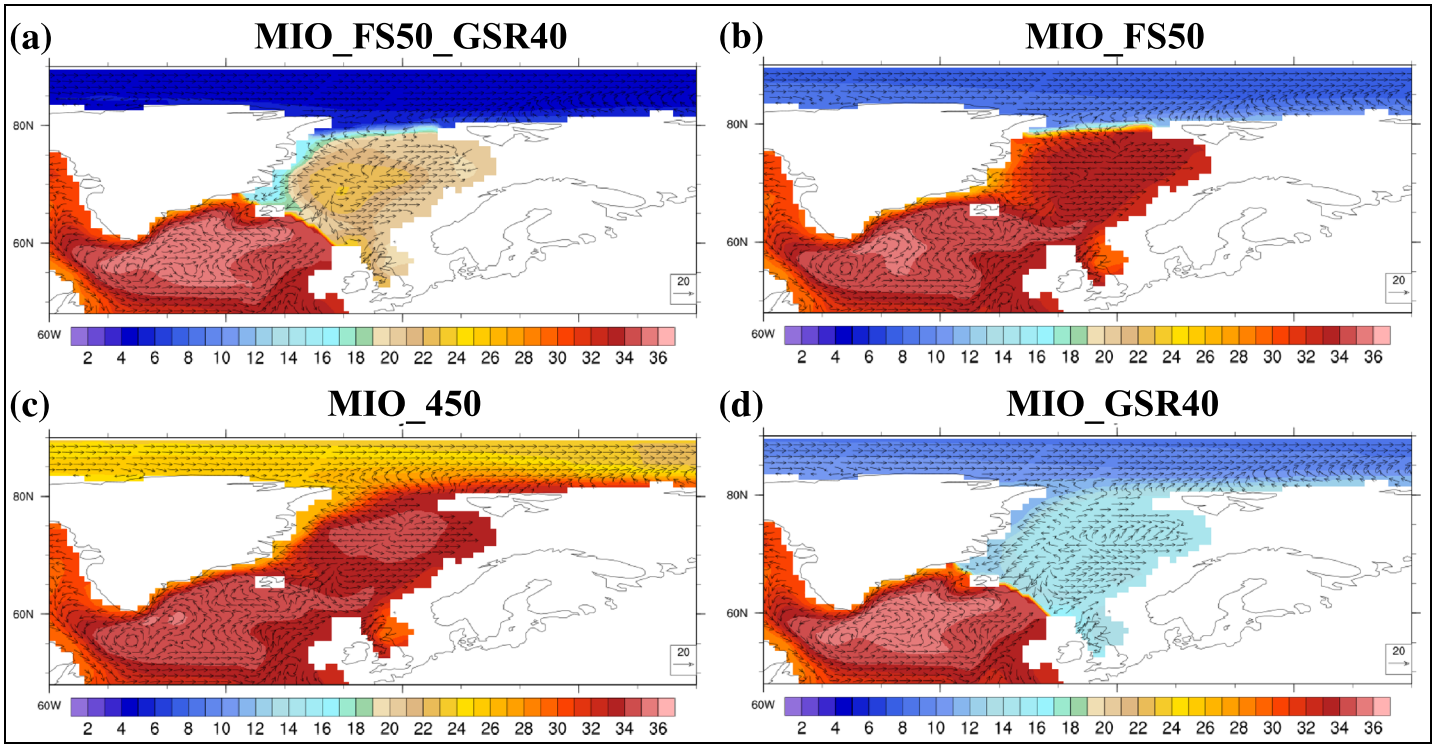

Figure 2. Salinity (in psu) and ocean velocity (cm/s) maps at the water depths of 50 m for the experiments of (a) MIO_FS50_GSR40, (b) MIO_FS50, (c) MIO_450, and (d) MIO_GSR40.

water from the Arctic returns south-westwards (surface to bottom layers) along the Greenland coast and south-eastwards at deeper layers (below ~500 m) (Figures 2a and 2b; Figures S1-S2a,b, S16). This deep overflow of dense, cold water results from newly established deep-water formation sites north of Iceland. Due to enhanced inflow of salty waters and enhanced freshwater export of Arctic origin across the GSR, the Arctic Ocean starts to become more saline. Nevertheless, there is a pronounced salinity difference between the Nordic Seas and the Arctic Ocean due to the restricted exchange across a shallow FS gateway.

As NADW is formed at cooler temperatures, the associated cooling in the deep ocean (Figure 4b) and upwelling of deep waters to the Southern Ocean surface causes a cooling in the southern high latitudes (Figures 3 and 4), which is additionally boosted by enhanced westerlies (Figure 6a). As a consequence, deepening the

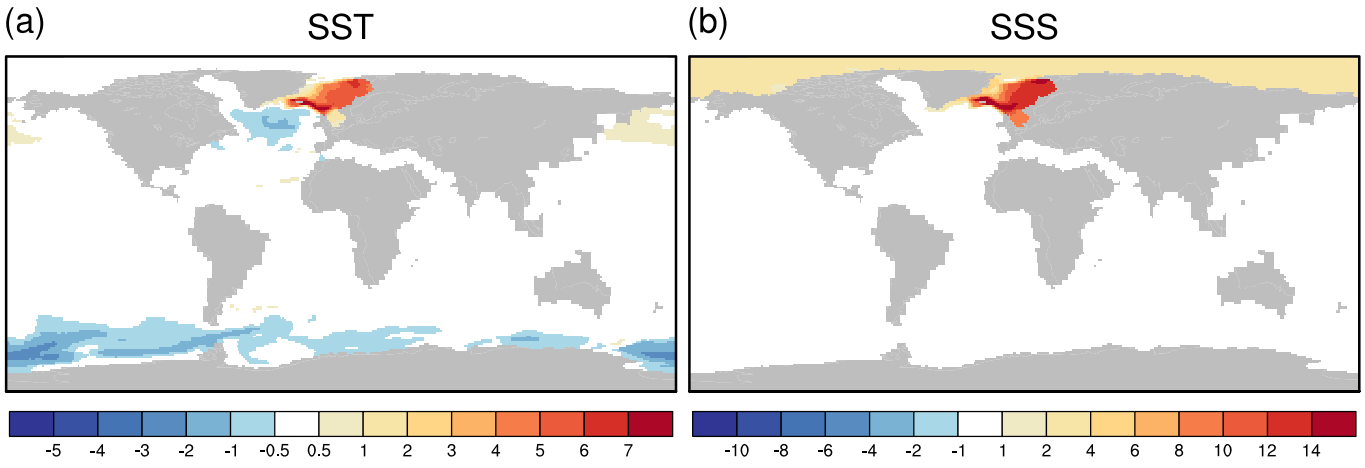

Figure 3. The effect of $\Delta GSR\_FS_{shallow}$ on (a) sea surface temperature anomalies (SST; in K) and (b) sea surface salinity anomalies (SSS; in psu).

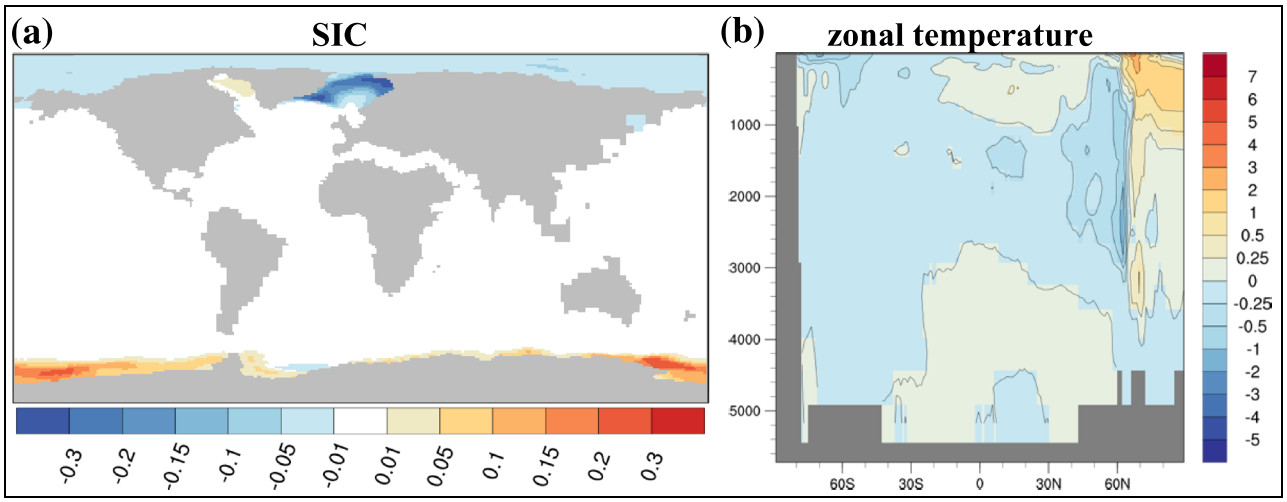

Figure 4. (a) Sea ice concentration changes and (b) zonal mean temperature anomalies (in K) in the Atlantic Ocean for scenario $\Delta GSR\_FS_{shallow}$.

GSR sill generates a cooling of up to −3 K in the Southern Ocean. This is accompanied by increase in perennial sea ice cover as detected in the Ross Sea (Figure 4a).

By means of three additional sensitivity experiments (listed in Table S1), we simulate the progressive deepening of GSR by stepwise changes from 40 to 500 mbsl for a shallow FS. The associated subscenarios to $\Delta GSR\_FS_{shallow}$ ($\Delta GSR_{100}\_FS_{shallow}$, $\Delta GSR_{300}\_FS_{shallow}$, and $\Delta GSR_{500}\_FS_{shallow}$; Table S2) show the same basic characteristics with stronger magnitudes of change for a deeper GSR sill (please see Appendix A for further details).

Similar to our scenario $\Delta GSR\_FS_{shallow}$, Stärz et al. (2017) found cooling (up to −2 K) south of the GSR. In the Nordic Seas, a warming (up to +10 K) and a salinity increase (up to +18 psu) are observed. Furthermore, an identical warming (up to +2 K) but stronger salinity increase (up to +14 psu) are detected in the Arctic Ocean. In contrast to our scenarios $\Delta GSR\_FS_{shallow}$, they found a warming (up to +4 K) in the Southern Ocean, while we observe a cooling (please see section 3.3 for further details).

3.2. Singular Effect of FS Deepening for a Deep GSR (ΔFS_GSR_{deep})

An isolated subsidence of the FS from a shallow depth of 50 mbsl toward a fully developed FS depth of ~2,500 mbsl for a deep GSR (~960 mbsl; ΔFS_GSR_{deep}) provides enhanced Atlantic water inflow to the polar/subpolar Arctic and unrestricted water exchange (Figures 2b and 2c). In the south of Iceland, temperatures and salinity remain unchanged at the surface (Figure 7), but a subsurface cooling (up to −2 K) is observed (Figure 8b), linked with southward advection of cold water from the Arctic Ocean.

Subsidence of the FS provides enhanced circulation (Figures 9b and 9c) of saltier and warmer water from the Atlantic Ocean into the Nordic Seas and Arctic Ocean. We detect a warming (up to +3 K) and a salinity increase (up to +6 psu) in the Nordic Seas that are less pronounced than in $\Delta GSR\_FS_{shallow}$. In the Arctic, temperatures remain unaltered at the surface, but warming (up to +6 K) in subsurface water, associated with reduced sea ice cover and a stronger salinity increase (up to +15 psu), is detected (Figures 7 and 8). The circulation across the FS is characterized by a relatively saline and warm water that is transported north-eastwards in the near-surface/subsurface layers (upper ~900 m) and at the deepest layers (below ~1,500 m). Cold but fresher water from the Arctic Ocean returns southwards in the near-surface layers (upper ~300 m) along the East Greenland coast and at deeper layers (between 900 and 1,500 mbsl) (Figures 2b and 2c; Figures S1; S3b,c). Due to the bulk inflow of southern source Atlantic water, the Arctic Ocean becomes more saline.

The strong salinity increase in the Arctic Ocean increases the density of NADW by entrainment. This causes an enhanced contribution of NADW to the abyssal ocean (between 2,500 and 5,000 mbsl) (Figure 8c) and at the expense of the colder southern source water component (Figures 9b and 9c). The global AABW index, as defined by the meridional circulation in the Southern Ocean between 60°S and 80°S, decreases by up to

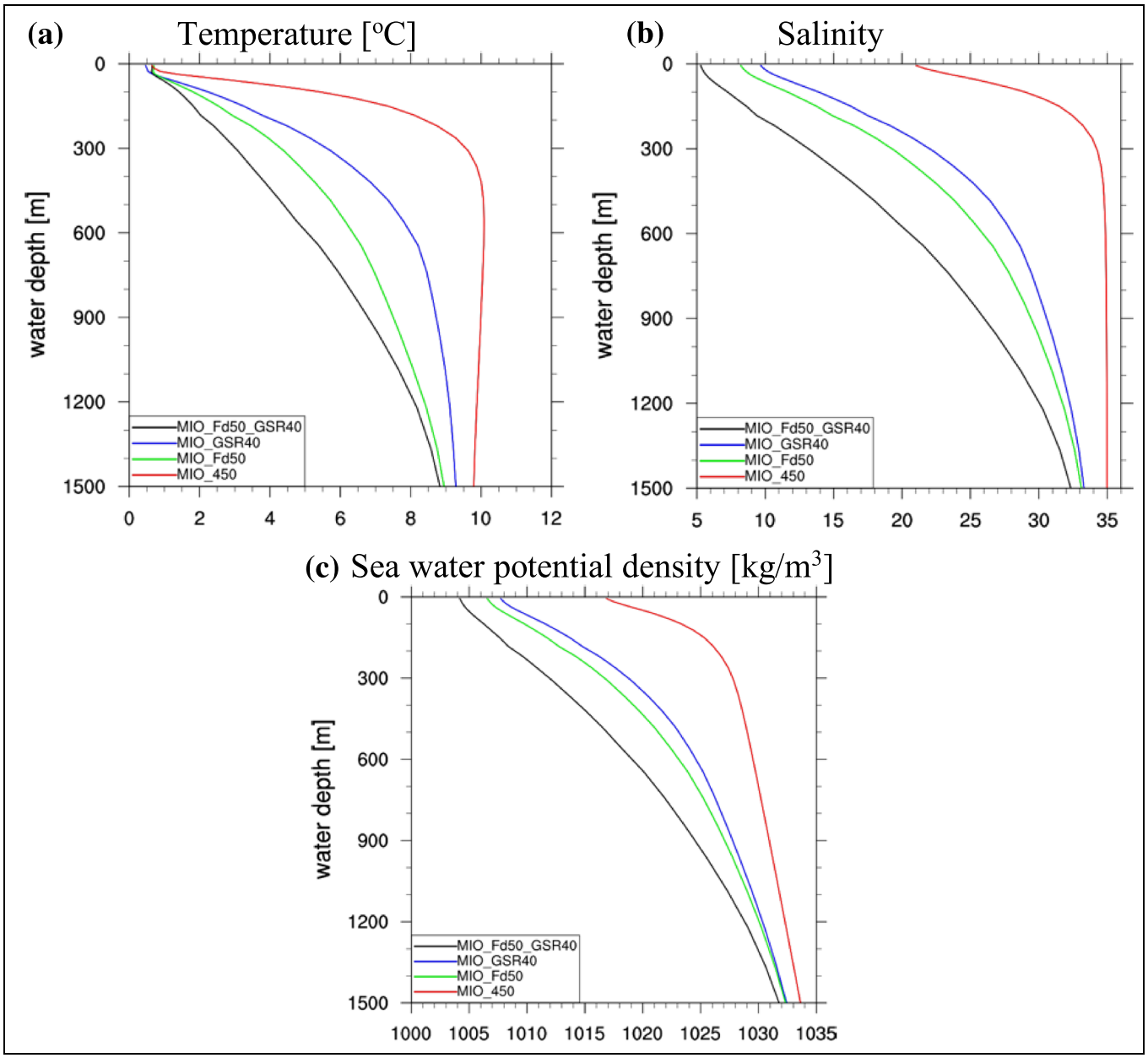

Figure 5. Evolution of (a) temperature (in °C), (b) salinity (in psu), and (c) density (in kg/m^3) profiles in the Arctic as a consequence of gateways changes.

−0.72 Sv (Figures 9b and 9c; Figure S3b,c; Table S3). A decrease in AABW formation linked with a weakening of westerlies (Figure 6b) decreases upwelling in the Antarctic coast (Figures 7a–8b). These relative changes largely counteract each other and cause a negligible warming in the upwelling regions of the Southern Ocean (Figure 7a). By using two additional experiments (Table S1), we consider the gradual subsidence of FS from 50 to 300 mbsl while GSR is already deep. In the model subscenarios $\Delta FS_{100}\_GSR_{deep}$ and $\Delta FS_{300}\_GSR_{deep}$ (Table S2), similar basic characteristics as in scenario ΔFS_GSR_{deep} are detected (please see Appendix A for further details).

3.3. Effect of ΔGSR_FS_{deep}, $\Delta FS\_GSR_{shallow}$, and $\Delta GSR\_\Delta FS$

First, in comparison to the previous scenario $\Delta GSR\_FS_{shallow}$, we alternatively consider the impact of the GSR deepening for a deep FS sill (~2,500 mbsl) in scenario ΔGSR_FS_{deep} (Table 2). The deep FS sill in

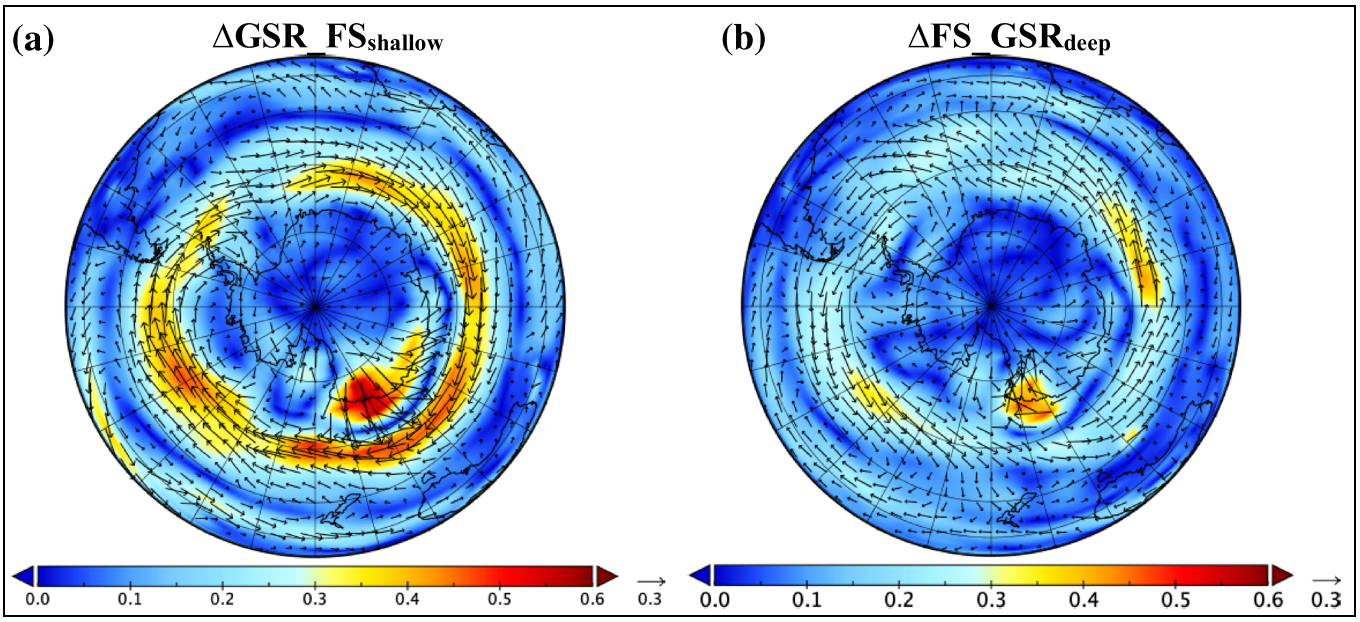

Figure 6. Change of annual mean wind (m/s) in the Southern Hemisphere for (a) $\Delta GSR\_FS_{shallow}$ and (b) ΔFS_GSR_{deep}.

ΔGSR_FS_{deep} enables the inflow of saline Atlantic water to the Arctic Ocean (Figures 2c and 2d; Figure S2) upon the deepening of the GSR. Furthermore, a modern prototype circulation across the GSR as simulated in Stärz et al. (2017) is established in ΔGSR_FS_{deep}. Temperature and salinity changes south of Iceland are similar to $\Delta GSR\_FS_{shallow}$, but warming (up to +10 K) and salinity increase (up to +17 psu) in the Nordic Seas (Figure 10) are more pronounced in ΔGSR_FS_{deep}. In the Arctic, temperature remains unaltered at the surface, but a stronger salinity increase (up to +14 psu) is detected. These Northern Hemisphere thermohaline changes in ΔGSR_FS_{deep} are similar to Stärz et al. (2017), although the Barents Sea region is subaerially exposed in our setup. By using three additional experiments (Table S1), we simulate the gradual subsidence of GSR by stepwise changes from 40 to 150 mbsl while FS is already deep. The associated subscenarios $\Delta GSR_{50}\_FS_{deep}$, $\Delta GSR_{80}\_FS_{deep}$, and $\Delta GSR_{150}\_FS_{deep}$ (Table S2) show similar basic characteristics as in scenario ΔGSR_FS_{deep} (please see Appendix A for further details).

In the following, we consider the impact of FS deepening for a shallow GSR sill depth (40 mbsl) ($\Delta FS\_GSR_{shallow}$) as an alternative scenario to ΔFS_GSR_{deep}. Temperatures and salinity remain largely unaltered south of Iceland (Figure 11). In the Nordic Seas, a salinity decrease (up to −6 psu) and cooling

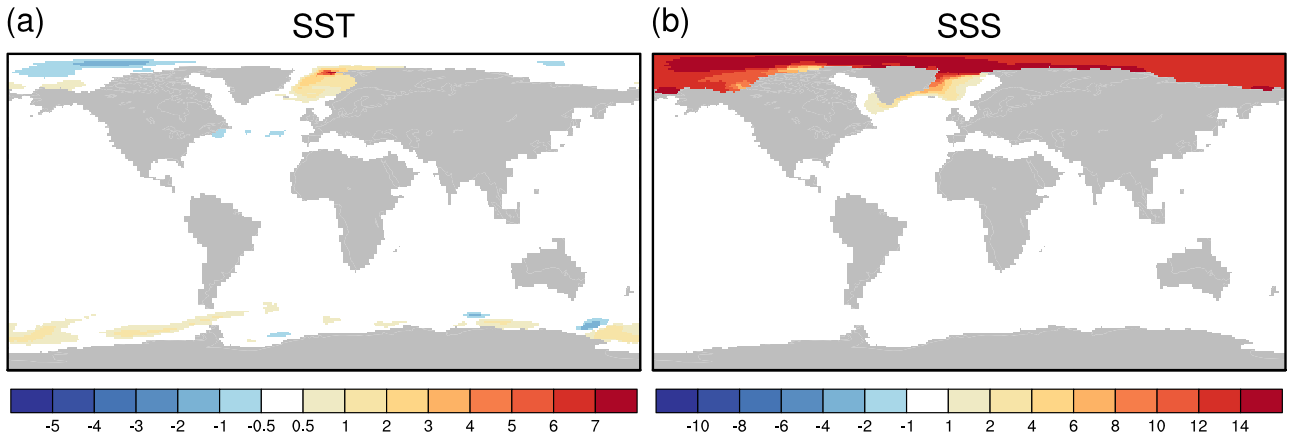

Figure 7. Same as Figure 3, but for ΔFS_GSR_{deep}.

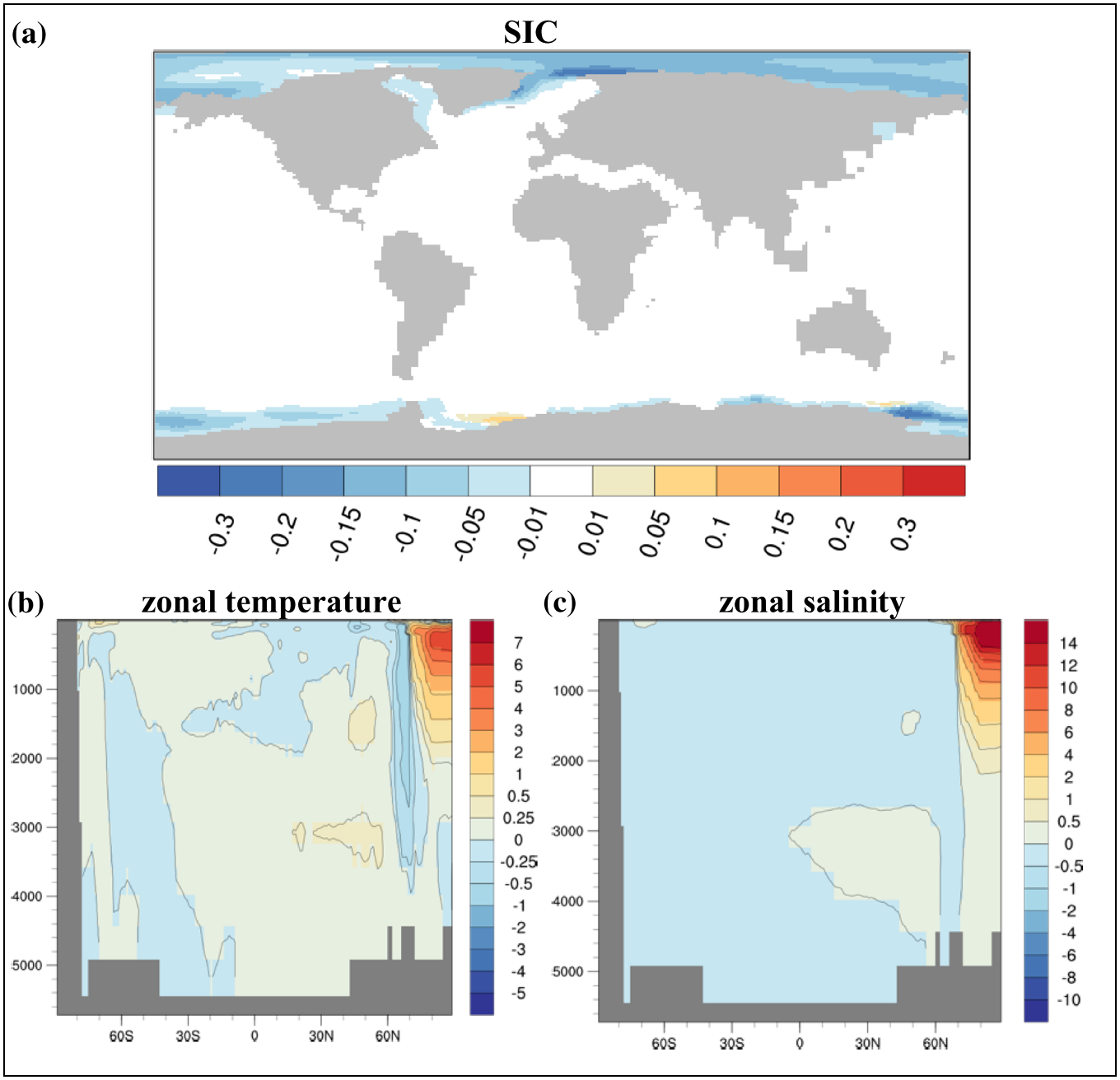

Figure 8. (a) Sea ice concentration changes, (b) zonal mean temperature anomalies (in K), and (c) zonal mean salinity anomalies (in psu) in the Atlantic Ocean for ΔFS_GSR_{deep}.

(up to −1 K) is detected, in contrast to the simulated salinity increase and warming in ΔFS_GSR_{deep}. In the Arctic Ocean, temperature remains largely unaltered as in ΔFS_GSR_{deep}, but a less pronounced salinity increase (up to +5 psu) is detected and an anomalous salinity dipole between the Arctic Ocean and Nordic Seas is established (Figure 11). This salinity anomaly is linked to ingress of salty waters to the Arctic Ocean and enhanced freshwater export of Arctic origin across the FS. We simulate the gradual subsidence of FS from 50 to 500 mbsl while GSR is shallow by using three additional experiments (listed in Table S1). The associated subscenarios $\Delta FS_{100}\_GSR_{shallow}$, $\Delta FS_{300}\_GSR_{shallow}$, and $\Delta FS_{500}\_GSR_{shallow}$ (Table S2) provide the same basic characteristics with stronger magnitudes of change for a deeper FS sill (please see Appendix A for further details).

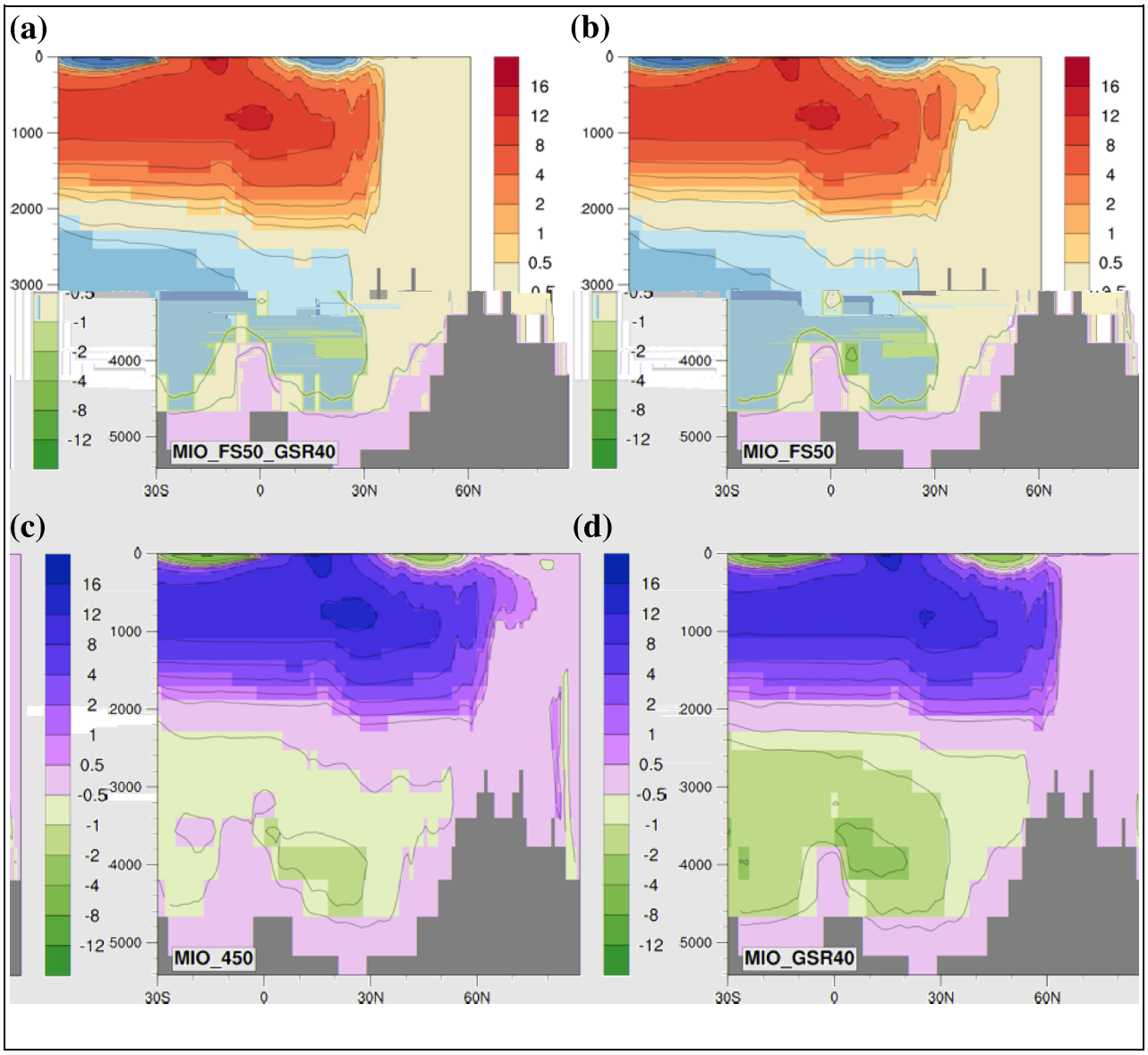

Figure 9. Atlantic Meridional Overturning Circulation (AMOC; in Sv) for (a) MIO_FS50 _GSR40, (b) MIO_FS50, (c) MIO_450, and (d) MIO_GSR40.

Finally, we consider the combined FS deepening from 50 to ~2,500 mbsl and GSR deepening from 40 to ~960 mbsl in model scenario ΔGSR_ΔFS (Figures 12a and 12b). The deep sills enable unrestricted ocean water exchange across both gateways at the same time. The resulting thermohaline characteristics have the strongest concurrence to ΔGSR_FS_{deep}, which highlights the importance of the GSR deepening as the dominant control factor. In the Arctic, temperature remains unaltered, but a more pronounced salinity increase (up to +20 psu) than in $\Delta GSR\_FS_{shallow}$ and ΔGSR_FS_{deep} is detected. Furthermore, the temperature change in the Nordic Seas (up to +8 K) in ΔGSR_ΔFS is within the range of these two scenarios. By means of three different model sensitivity experiments (Table S1), we examine the combined deepening of GSR from 40 to 500 mbsl and FS deepening from 50 to 500 mbsl at the same time by stepwise changes. The associated subscenarios to ΔGSR_ΔFS ($\Delta GSR_{100}\_\Delta FS_{100}$, $\Delta GSR_{300}\_\Delta FS_{300}$, and $\Delta GSR_{500}\_\Delta FS_{500}$; Table S2) show the similar basic characteristics with stronger magnitudes of change for a deeper GSR and FS sill (please see Appendix A for further details).

In order to analyze the synergy effect of combined GSR and FS deepening (from shallow conditions), we adapt a factor separation analysis (Stein & Alpert, 1993). According to this analysis, the synergy (ΔSYN)

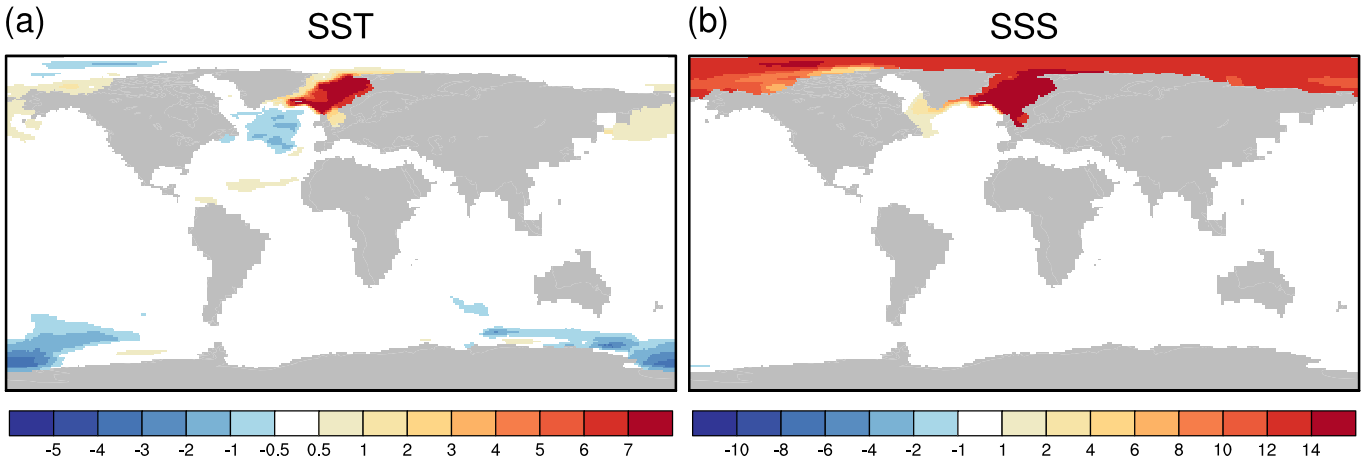

Figure 10. Same as Figure 3, but for ΔGSR_FS_{deep}.

can be expressed by the difference of the combined sill deepening effect (ΔGSR_ΔFS) and the singular effects ΔGSR and ΔFS (Figures 12c and 12d). The synergetic effects show a warming in the Nordic Seas, which in fact should be interpreted as cooling effect of FS deepening for a shallow GSR ($\Delta FS\_GSR_{shallow}$; Figure 11a). However, this cooling effect turns into a warming signature for a FS deepening once the GSR is already deep (ΔFS_GSR_{deep}; Figure 7a). Similarly, the salinity dipole with a Nordic Sea decrease and Arctic increase in ΔFS (FS deepening) is only established while the GSR is shallow ($\Delta FS\_GSR_{shallow}$; Figure 11b). In that sense, the dipole mainly represents a redistribution of salinity across the FS, but the combined mean salinity is almost constant (~24 psu). In contrast, once the GSR is already deep, the FS deepening enables a net salinity increase in the Nordic Seas and Arctic Ocean (up to +15 psu, Figure 7b), which explains the strong positive salinities in ΔSYN.

4. Discussion

During the Cenozoic, the Arctic Ocean changes from a restricted freshwater regime toward a more saline modern ocean. These massive oceanographic changes are argued to be driven by the subsidence of the GSR (Stärz et al., 2017) and opening of FS (Jakobsson et al., 2007; Thompson et al., 2012). The evolution of a landlocked Arctic Ocean to a fully ventilated ocean regime, characterized by a warmer ocean with higher salinities (Thompson et al., 2012; Waddell & Moore, 2008), initiated at ~18.2 Ma as a consequence of the opening/deepening of the FS (Ehlers & Jokat, 2013; Jakobsson et al., 2007; Moran et al., 2006). Previous studies (i.e., Jakobsson et al., 2007; Thompson et al., 2012) suggested that the FS was narrower than the width we have considered in order to induce ventilation of the Arctic Ocean. Given a rotational control

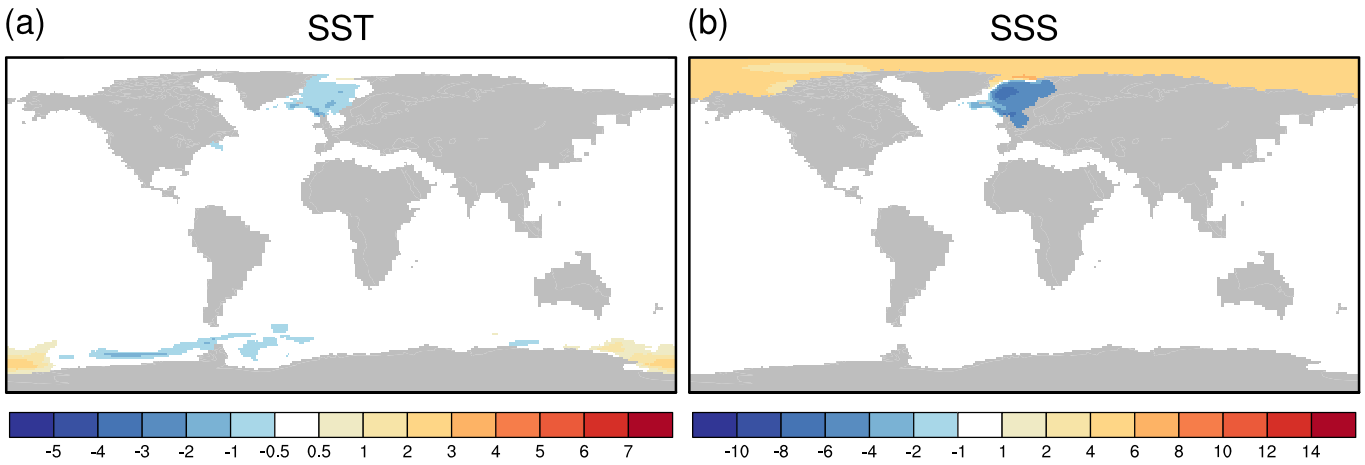

Figure 11. Same as Figure 3, but for $\Delta FS\_GSR_{shallow}$.

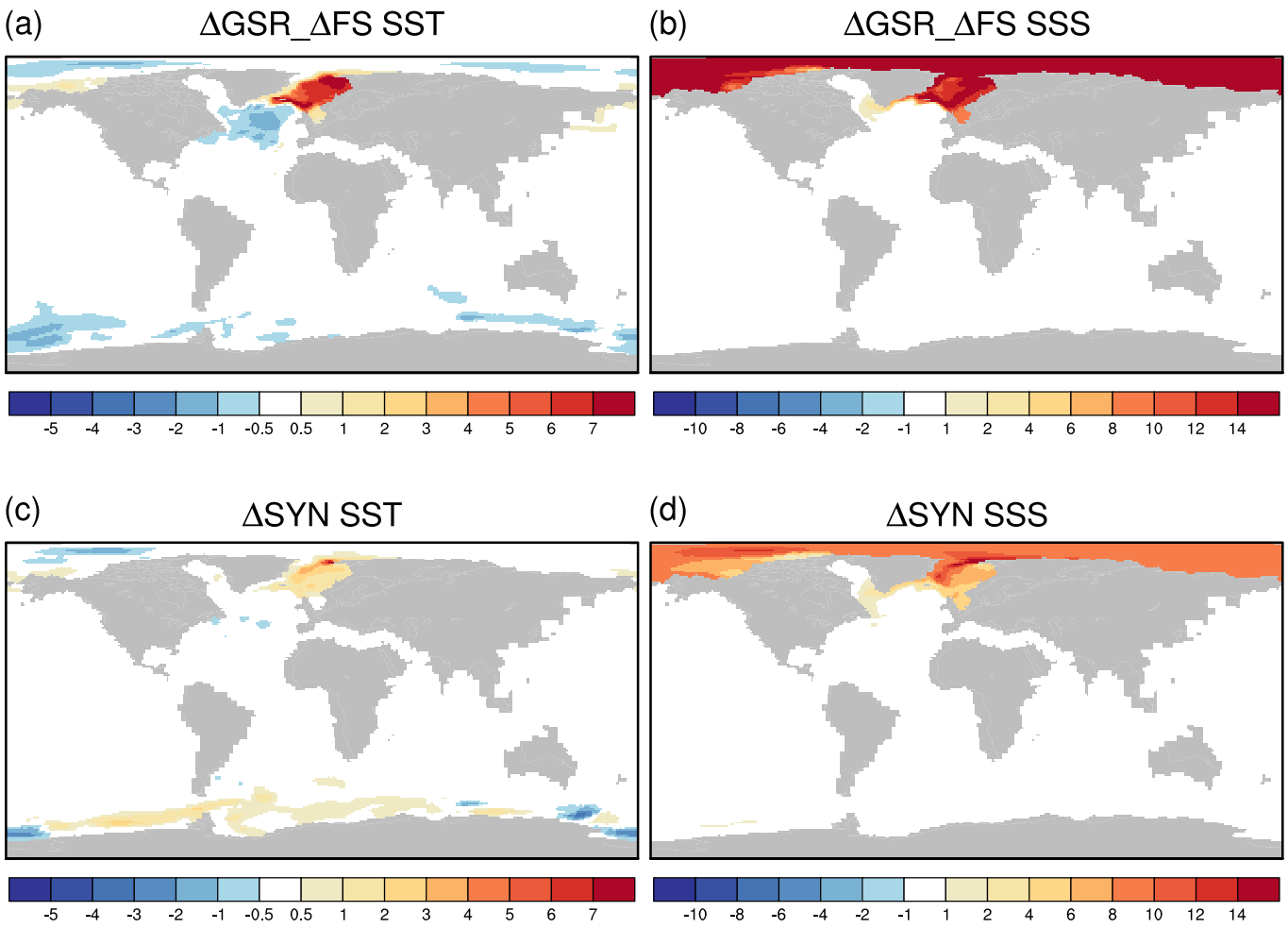

Figure 12. Same as Figure 3, but for ΔGSR_ΔFS (a, b) and the application of a synergy analysis between gateways changes (c, d).

for widths of a more than ~50 km (Thompson et al., 2012), we expect that the dynamic control for widths less than this represents a hydraulic regime. Hence, from the point of ventilation, we do not expect a big difference to Jakobsson et al. (2007) and Thompson et al. (2012) if we would apply similar widths.

The progressive deepening of both Nordic gateways permits increased export of NADW to the abyssal ocean during the Miocene. This agrees with the findings of previous studies (Knies et al., 2014; Poore et al., 2006). Transformation of these water masses associated with mixing and upwelling to the Southern Ocean surface cause a negligible warming in the southern high latitudes (Figure 7a) (Gordon, 1981; Wright & Miller, 1996). Warmer water temperatures and reduction of sea ice cover along the Antarctic coast of Southern Ocean, leading to an overall reduction in AABW production (Huang et al., 2017), are detected in ΔFS_GSR_{deep} (FS deepening for a deep GSR sill depth). In contrast, during the mid-Miocene (~ 15.6 Ma), an increase in AABW production is found in the oxygen and carbon isotopes retrieved from deep-sea drill sites (Flower & Kennett, 1995; Wright & Miller, 1996), which supports the results of $\Delta GSR\_FS_{shallow}$ (GSR deepening for a shallow FS) (Figures 9a and 9b). Sea surface cooling around the Antarctic coastline is linked to an increase in sea ice extent and the associated ice-albedo feedback (Huang et al., 2017). Previous investigation by von der Heydt and Dijkstra (2006) using the Community Climate System Model (CCSM) version 1.4 simulated Miocene (~20 Ma) conditions with fresher Nordic Seas than the Arctic Ocean, in agreement with the salinity dipole found in our $\Delta FS\_GSR_{shallow}$ (FS deepening for a shallow GSR) scenario.

4.1. Geological Constraints and Model Scenarios

Seismic reflection profiles of Reykjanes Ridge (south of Iceland) show the evolution of Icelandic mantle plume activity back to 55 Ma (Parnell-Turner et al., 2014). Seismic profiles indicate a strong decline

(tectonic dormancy) in Icelandic mantle plume activity between ~55 and 36 Ma, but still with a subaerial Reykjanes Ridge at the end of this period. The GSR gateway started to form already around 36 Ma (Davies et al., 2001; Laberg et al., 2005; Stärz et al., 2017). At the time of GSR sill deepening, Svalbard was very close to North East Greenland (Ehlers & Jokat, 2013). With time, the FS gateways formed and widened as a consequence of a large strike-slip movement between Greenland and Svalbard. The geophysical data in the FS (Jokat et al., 2016) provide sound constraints that at the time when GSR deepening initiated, the FS was shallow.

The subsequent opening of FS is relatively well constrained by magnetic data that show initial oceanic crust within the FS might have been formed between 24 and 21 Ma (Jokat et al., 2016). Seismic studies in the northern North Atlantic and Chukchi Plateau, central Arctic Ocean, support the scenario that a restricted shallow water exchange between the northern North Atlantic and the Arctic Ocean is likely in this time period (Hegewald & Jokat, 2013; Jokat et al., 2008). From ~24 Ma onwards, the FS becomes deeper and wider (Ehlers & Jokat, 2013).

Further south, GSR sill is already well below sea level (below ~300 m) between ~20 and 24 Ma (Stärz et al., 2017). In combination, geological evidence and our results suggest a singular subsidence of GSR toward a deep gateway configuration for a shallow FS ($\Delta GSR\_FS_{shallow}$) is a likely scenario for the time period of around 20 ± 3 Ma (Hegewald & Jokat, 2013; Jokat et al., 2008, 2016; Stärz et al., 2017).

Jokat et al. (2008) suggest from analyzing seismic data across the Yermak Plateau that a shallow water exchange between the Nordic Seas and the Arctic Ocean already existed well before establishment of a deep-water passage in the FS. The interpretation of magnetic and seismic data reveals that the formation of oceanic crust likely initiated in the FS at ~21 Ma (Jokat et al., 2016). A paleobathymetric model based on these regional seismic and magnetic data shows that a deep-water exchange between the Nordic Seas and the Arctic Ocean was likely between 17 and 20 Ma (Ehlers & Jokat, 2013). As the formation of oceanic crust initiated at ~21 Ma, the FS deepened to sill depths greater than 1,500 mbsl at around 17 Ma. Scientific drilling indicates a fully ventilated Arctic Ocean from 18.2 Ma onwards allowing an unrestricted exchange of deep Arctic water and warm Atlantic water (Jakobsson et al., 2007; Moran et al., 2006). Further, progressive deepening of the GSR sill allowed increased outflow of NADW to the Atlantic Ocean through late Miocene (Knies et al., 2014; Poore et al., 2006). Therefore, subsidence of the FS from a shallow depth toward a fully developed FS depth for a deep GSR (ΔFS_GSR_{deep}) would be the likely scenario for time period younger than 18 Ma (Ehlers & Jokat, 2013; Jokat et al., 2008; Stärz et al., 2017).

In summary, from the geophysical/geological data, we deduce that the scenarios of ΔGSR_FS_{deep}, $\Delta FS\_GSR_{shallow}$, and $\Delta GSR\_\Delta FS$ are three unlikely configurations from a tectonic point of view considering relative timing of subsidence of both gateways. Therefore, we suggest the most likely scenarios that provide fingerprints of characteristic thermohaline changes based on geological evidence and tectonic constraints are as follows: Phase 1: GSR sill gradual subsidence toward a deep gateway configuration for a shallow FS sill depth ($\Delta GSR\_FS_{shallow}$) at around 20 ± 3 Ma (Jokat et al., 2016) and Phase 2: the opening of FS initiated when GSR is already deeper than ~300 m (ΔFS_GSR_{deep}) between ~20 and 24 Ma (Stärz et al., 2017).

5. Conclusions

By applying the climate model COSMOS, we have analyzed the impact of GSR and FS subsidence on the ocean circulation and climate during early to middle Miocene in different model scenarios. The subsidence of GSR and FS enables enhanced circulation of saltier and warmer water from the Atlantic Ocean into the Nordic Seas and Arctic Ocean that induces a salinization process in this region. Deepening of the GSR causes warming and a salinity increase in the Nordic Sea/Arctic Ocean and cooling in the southern high latitudes. These fingerprints of characteristic thermohaline changes in response to the GSR deepening are independent of the FS state. Furthermore, deepening of the FS gateway for a deep GSR causes less pronounced warming and salinity increase in the Nordic Seas. In contrast, unchanged temperatures and a stronger salinity increase in the Arctic and a negligible warming in the upwelling regions of the Southern Ocean are detected in our model simulations. Considering the impact of the gateways' subsidence, the GSR deepening is the dominant controlling factor for thermohaline changes.

Based on the geological/geophysical constraints, we conjecture that a tectonic situation with a progressive GSR deepening for a shallow FS sill depth configuration is the most likely Eocene to Miocene scenario (ΔGSR_FS$_{shallow}$). The deepening of FS initiated when GSR was already becoming deep (ΔFS_GSR$_{deep}$). In contrast, deepening of the FS for a shallow GSR (ΔFS_GSR$_{shallow}$) and GSR deepening while the FS is already deep (ΔGSR_FS$_{deep}$), as well as the combined deepening of both gateways at the same time (ΔGSR_ΔFS), are unlikely scenarios.

Future data from upcoming drilling projects can use our scenarios and these characteristic thermohaline changes as basis for various interpretation models to test and further our understanding of the high-latitude climate evolution by superposed gateway changes.

Appendix A: Effect of GSR and FS Deepening at Different Sill Depths (Subscenarios)

An isolated subsidence of GSR from 40 to 500 mbsl by stepwise changes for a shallow FS (ΔGSR$_{100}$_FS$_{shallow}$, ΔGSR$_{300}$_FS$_{shallow}$, and ΔGSR$_{500}$_FS$_{shallow}$; Table S2) shows the same basic characteristics in salinity as ΔGSR_FS$_{shallow}$ with stronger magnitudes of change for a deeper GSR sill (Figure S5). The sea surface temperature changes in the North Atlantic/Arctic appear to steadily become stronger with increasing sill depths. In the model subscenario ΔGSR$_{100}$_FS$_{shallow}$, we observe a strong cooling (up to −4 K) in the Southern Ocean (Figure S4). On the other hand, in ΔGSR$_{300}$_FS$_{shallow}$ and ΔGSR$_{500}$_FS$_{shallow}$, we detect less pronounced cooling (up to −2 K) in the Southern Ocean.

By means of two different model sensitivity experiments (Table S1), we consider the gradual subsidence of FS from 50 to 300 mbsl while GSR is already deep. The associated subscenarios to ΔFS_GSR$_{deep}$ (ΔFS$_{100}$_GSR$_{deep}$ and ΔFS$_{300}$_GSR$_{deep}$) show similar basic characteristics in salinity with stronger magnitudes of change for a deeper FS sill (Figure S7). In the model subscenario ΔFS$_{100}$_GSR$_{deep}$, we detect minor warming (up to +1 K) in the Nordic Seas and cooling (up to −2 K) in the Arctic Ocean. On the other hand, in ΔFS$_{300}$_GSR$_{deep}$, we observe warming (up to +2 K) in the Nordic Seas and a negligible cooling (up to −1 K) in the Arctic Ocean. We also observe a negligible warming in the upwelling regions of the Southern Ocean (Figure S6).

We simulate the gradual subsidence of GSR by stepwise changes from 40 to 150 mbsl while FS is already deep in three subscenarios (ΔGSR$_{50}$_FS$_{deep}$, ΔGSR$_{80}$_FS$_{deep}$, and ΔGSR$_{150}$_FS$_{deep}$). They show similar basic characteristics as in scenario ΔGSR_FS$_{deep}$ discussed in section 3.3 (Figures S8 and S9).

The associated subscenarios to ΔFS_GSR$_{shallow}$ (discussed in Section 3.3; ΔFS$_{100}$_GSR$_{shallow}$, ΔFS$_{300}$_GSR$_{shallow}$ and ΔFS$_{500}$_GSR$_{shallow}$) provide the same basic characteristics with stronger magnitudes of change for a deeper FS sill (Figures S10 and S11).

By using three different subscenarios (ΔGSR$_{100}$_ΔFS$_{100}$, ΔGSR$_{300}$_ΔFS$_{300}$, and ΔGSR$_{500}$_ΔFS$_{500}$), we examine the combined deepening of GSR from 40 to 500 mbsl and FS deepening from 50 to 500 mbsl at the same time by stepwise changes. They show the similar basic characteristics in salinity (Figure S12). In the model subscenario ΔGSR$_{100}$_ΔFS$_{100}$, we observe a weak warming (up to +1 K) in the Nordic Seas and unaltered Arctic Ocean (Figure S13). On the other hand, in ΔGSR$_{300}$_ΔFS$_{300}$, we detect warming (up to +4 K) in the Nordic Seas and cooling (up to −1 K) in the Arctic Ocean. We also observe a stronger cooling (up to −5 K) in the Southern Ocean (Figure S12). Again, in ΔGSR$_{500}$_ΔFS$_{500}$, we observe a stronger warming (up to +6 K) in the Nordic Seas and a little cooling in the Arctic Ocean. We detect a threshold in temperature for subscenario ΔGSR$_{300}$_ΔFS$_{300}$ (Figure S13).

Data Availability Statement

Data from this study are available for further use at https://doi.pangaea.de/10.1594/PANGAEA.915548 and additional data can be obtained from A.H. (akil.hossain@awi.de). The standard model code of the "COSMOS" (Community Earth System Models) version COSMOS-landveg r2413 is available upon request from the Max Planck Institute (MPI) for Meteorology in Hamburg (https://www.mpimet.mpg.de).

Conflict of Interest

The authors declare no conflict of interest.

Acknowledgments

This study is supported through institutional funds of the Helmholtz Centre for Polar and Marine Research through Work Package 3.2 (Earth system on tectonic time scales: From greenhouse to icehouse world) of its research program PACES-II.

References

Aagaard, K., & Carmack, E. C. (1994). The Arctic Ocean and climate: A perspective. In O. M. Johannessen, R. D. Muench, & J. E. Overland (Eds.), *The polar oceans and their role in shaping the global environment, Geophysical Monograph Series*, *Geophysical Monograph Series*, (Vol. 85, pp. 5–20). Washington, DC: American Geophysical Union. https://doi.org/10.1029/GM085

Bartoli, G., Sarnthein, M., Weinelt, M., Erlenkeuser, H., Garbe-Schönberg, D., & Lea, D. W. (2005). Final closure of Panama and the onset of northern hemisphere glaciation. *Earth and Planetary Science Letters*, *237*(1–2), 33–44. https://doi.org/10.1016/j.epsl.2005.06.020

Broecker, W. S., & Denton, G. H. (1989). The role of ocean-atmosphere reorganizations in glacial cycles. *Geochimica et Cosmochimica Acta*, *53*(10), 2465–2501. https://doi.org/10.1016/0016-7037(89)90123-3

Butt, F. A., Drange, H., Elverhøi, A., Otterå, O. H., & Solheim, A. (2002). Modelling Late Cenozoic isostatic elevation changes in the Barents Sea and their implications for oceanic and climatic regimes: Preliminary results. *Quaternary Science Reviews*, *21*(14–15), 1643–1660. https://doi.org/10.1016/S0277-3791(02)00018-5

Davies, R., Cartwright, J., Pike, J., & Line, C. (2001). Early Oligocene initiation of North Atlantic Deep Water formation. *Nature*, *410*(6831), 917–920. https://doi.org/10.1038/35073551

Ehlers, B. M., & Jokat, W. (2013). Paleo-bathymetry of the northern North Atlantic and consequences for the opening of the Fram Strait. *Marine Geophysical Research*, *34*, 25–43. https://doi.org/10.1007/s11001-013-9165-9

Elsworth, G., Galbraith, E., Halverson, G., & Yang, S. (2017). Enhanced weathering and CO_2 drawdown caused by latest Eocene strengthening of the Atlantic meridional overturning circulation. *Nature Geoscience*, *10*(3), 213–216. https://doi.org/10.1038/ngeo2888

Flower, B. P., & Kennett, J. P. (1995). Middle Miocene deepwater paleoceanography in the southwest Pacific: Relations with East Antarctic Ice Sheet development. *Paleoceanography*, *10*(6), 1095–1112. https://doi.org/10.1029/95PA02022

Gong, X., Knorr, G., Lohmann, G., & Zhang, X. (2013). Dependence of abrupt Atlantic meridional ocean circulation changes on climate background states. *Geophysical Research Letters*, *40*, 3698–3704. https://doi.org/10.1002/grl.50701

Gordon, A. L. (1981). Seasonality of Southern Ocean sea ice. *Journal of Geophysical Research*, *86*(C5), 4193–4197. https://doi.org/10.1029/JC086iC05p04193

Haug, G. H., & Tiedemann, R. (1998). Effect of the formation of the Isthmus of Panama on Atlantic Ocean thermohaline circulation. *Nature*, *393*(6686), 673–676. https://doi.org/10.1038/31447

Hegewald, A., & Jokat, W. (2013). Relative sea level variations in the Chukchi region-Arctic Ocean-since the late Eocene. *Geophysical Research Letters*, *40*, 803–807. https://doi.org/10.1002/GRL.50182

Herold, N., Seton, M., Müller, R. D., You, Y., & Huber, M. (2008). Middle Miocene tectonic boundary conditions for use in climate models. *Geochemistry, Geophysics, Geosystems*, *9*, Q10009. https://doi.org/10.1029/2008GC002046

von der Heydt, A., & Dijkstra, H. A. (2006). Effect of ocean gateways on the global ocean circulation in the late Oligocene and early Miocene. *Paleoceanography*, *21*, PA1011. https://doi.org/10.1029/2005PA001149

Huang, X., Gohl, K., & Jokat, W. (2014). Variability in Cenozoic sedimentation and paleo-water depths of the Weddell Sea basin related to pre-glacial and glacial conditions of Antarctica. *Global and Planetary Change*, *118*, 25–41. https://doi.org/10.1016/j.gloplacha.2014.03.010

Huang, X., Stärz, M., Gohl, K., Knorr, G., & Lohmann, G. (2017). Impact of Weddell Sea shelf progradation on Antarctic bottom water formation during the Miocene. *Paleoceanography*, *32*, 304–317. https://doi.org/10.1002/2016PA002987

Hutchinson, D. K., Coxall, H. K., O'Regan, M., Nilsson, J., Caballero, R., & de Boer, A. M. (2019). Arctic closure as a trigger for Atlantic overturning at the Eocene-Oligocene transition. *Nature Communications*, *10*(1), 1–9.

Jakobsson, M., Backman, J., Rudels, B., Nycander, J., Frank, M., Mayer, L., et al. (2007). The early Miocene onset of a ventilated circulation regime in the Arctic Ocean. *Nature*, *447*(7147), 986–990. https://doi.org/10.1038/nature05924

Jokat, W., Geissler, W., & Voss, M. (2008). Basement structure of the north-western Yermak Plateau. *Geophysical Research Letters*, *35*, L05309. https://doi.org/10.1029/2007GL032892

Jokat, W., Lehmann, P., Damaske, D., & Nelson, J. B. (2016). Magnetic signature of North-East Greenland, the Morris Jesup Rise, the Yermak Plateau, the central Fram Strait: Constraints for the rift/drift history between Greenland and Svalbard since the Eocene. *Tectonophysics*, *691*, 98–109. https://doi.org/10.1016/j.tecto.2015.12.002

Jungclaus, J. H., Keenlyside, N., Botzet, M., Haak, H., Luo, J. J., Latif, M., et al. (2006). Ocean circulation and tropical variability in the coupled model ECHAM5/MPI-OM. *Journal of Climate*, *19*(16), 3952–3972. https://doi.org/10.1175/JCLI3827.1

Jungclaus, J. H., Lorenz, S. J., Timmreck, C., Reick, C. H., Brovkin, V., Six, K., et al. (2010). Climate and carbon-cycle variability over the last millennium. *Climate of the Past*, *6*(5), 723–737. https://doi.org/10.5194/cp-6-723-2010

Knies, J., & Gaina, C. (2008). Middle Miocene ice sheet expansion in the Arctic: Views from the Barents Sea. *Geochemistry, Geophysics, Geosystems*, *9*, Q02015. https://doi.org/10.1029/2007GC001824

Knies, J., Mattingsdal, R., Fabian, K., Grøsfjeld, K., Baranwal, S., Husum, K., et al. (2014). Effect of early Pliocene uplift on late Pliocene cooling in the Arctic–Atlantic gateway. *Earth and Planetary Science Letters*, *387*, 132–144. https://doi.org/10.1016/j.epsl.2013.11.007

Knorr, G., Butzin, M., Micheels, A., & Lohmann, G. (2011). A warm Miocene climate at low atmospheric CO_2 levels. *Geophysical Research Letters*, *38*, L20701. https://doi.org/10.1029/2011GL048873

Knorr, G., & Lohmann, G. (2014). Climate warming during Antarctic ice sheet expansion at the Middle Miocene transition. *Nature Geoscience*, *7*(5), 376–381. https://doi.org/10.1038/ngeo2119

Laberg, J. S., Stoker, M. S., Dahlgren, K. T., de Haas, H., Haflidason, H., Hjelstuen, B. O., et al. (2005). Cenozoic alongslope processes and sedimentation on the NW European Atlantic margin. *Marine and Petroleum Geology*, *22*(9–10), 1069–1088. https://doi.org/10.1016/j.marpetgeo.2005.01.008

Lohmann, G., Pfeiffer, M., Laepple, T., Leduc, G., & Kim, J. H. (2013). A model-data comparison of the Holocene global sea surface temperature evolution. *Climate of the Past*, *9*(4), 1807–1839. https://doi.org/10.5194/cp-9-1807-2013

Marsland, S. J., Haak, H., Jungclaus, J. H., Latif, M., & Röske, F. (2003). The Max-Planck-Institute global ocean/sea ice model with orthogonal curvilinear coordinates. *Ocean Modelling*, *5*(2), 91–127. https://doi.org/10.1016/S1463-5003(02)00015-X

Moran, K., Backman, J., Brinkhuis, H., Clemens, S. C., Cronin, T., Dickens, G. R., et al. (2006). The Cenozoic palaeoenvironment of the Arctic Ocean. *Nature*, *441*(7093), 601–605. https://doi.org/10.1038/nature04800

Parnell-Turner, R., White, N., Henstock, T., Murton, B., Maclennan, J., & Jones, S. M. (2014). A continuous 55-million-year record of transient mantle plume activity beneath Iceland. *Nature Geoscience*, *7*(12), 914–919. https://doi.org/10.1038/ngeo2281

Poore, H. R., Samworth, R., White, N. J., Jones, S. M., & McCave, I. N. (2006). Neogene overflow of northern component water at the Greenland-Scotland Ridge. *Geochemistry, Geophysics, Geosystems*, *7*, Q06010. https://doi.org/10.1029/2005GC001085

Pratt, L. J., & Spall, M. A. (2008). Circulation and exchange in choked marginal seas. *Journal of Physical Oceanography*, *38*(12), 2639–2661. https://doi.org/10.1175/2008JPO3946.1

Raddatz, T. J., Reick, C. H., Knorr, W., Kattge, J., Roeckner, E., Schnur, R., et al. (2007). Will the tropical land biosphere dominate the climate–carbon cycle feedback during the twenty-first century? *Climate Dynamics*, *29*(6), 565–574. https://doi.org/10.1007/s00382-007-0247-8

Roeckner, E., Bäuml, G., Bonaventura, L., Brokopf, R., Esch, M., Giorgetta, M., et al. (2003). The atmospheric general circulation model ECHAM 5. PART I: Model description. *Report/MPI für Meteorologie,* 349. http://hdl.handle.net/11858/00-001M-0000-0012-0144-5

Stärz, M., Jokat, W., Knorr, G., & Lohmann, G. (2017). Threshold in North Atlantic-Arctic Ocean circulation controlled by the subsidence of the Greenland-Scotland Ridge. *Nature Communications*, *8*, 15681. https://doi.org/10.1038/ncomms15681

Stärz, M., Lohmann, G., & Knorr, G. (2016). The effect of a dynamic soil scheme on the climate of the mid-Holocene and the Last Glacial Maximum. *Climate of the Past*, *12*(1), 151–170. https://doi.org/10.5194/cp-12-151-2016

Stein, R., Fahl, K., Schreck, M., Knorr, G., Niessen, F., Forwick, M., et al. (2016). Evidence for ice-free summers in the late Miocene central Arctic Ocean. *Nature Communications*, *7*, 11148. https://doi.org/10.1038/ncomms11148

Stein, U., & Alpert, P. I. N. H. A. S. (1993). Factor separation in numerical simulations. *Journal of the Atmospheric Sciences*, *50*(14), 2107–2115. https://doi.org/10.1175/1520-0469(1993)050<2107:FSINS>2.0.CO;2

Stepanek, C., & Lohmann, G. (2012). Modelling mid-Pliocene climate with COSMOS. *Geoscientific Model Development*, *5*(5), 1221–1243. https://doi.org/10.5194/gmd-5-1221-2012

Talwani, M., Udintsev, G., & White, S. M. (1976). *Initial Reports of the Deep Sea Drilling Project* (Vol. 38). Dublin, Ireland to Amsterdam, The Netherlands: US Government Printing Office.

Thiede, J., & Myhre, A. M. (1996). The palaeoceanographic history of the North Atlantic–Arctic gateways: Synthesis of the Leg 151 drilling results. In *Proceedings of the Ocean Drilling Program, Scientific Results* (Vol. 151, pp. 645–658). TX: Ocean Drilling Program College Station.

Thompson, B., Jakobsson, M., Nilsson, J., Nycander, J., & Döös, K. (2012). A model study of the first ventilated regime of the Arctic Ocean during the early Miocene. *Polar Research*, *31*, 10859. https://doi.org/10.3402/polar.v31i0.10859

Via, R. K., & Thomas, D. J. (2006). Evolution of Atlantic thermohaline circulation: Early Oligocene onset of deep-water production in the North Atlantic. *Geology*, *34*(6), 441–444. https://doi.org/10.1130/G22545.1

von Appen, W. J., Schauer, U., Somavilla, R., Bauerfeind, E., & Beszczynska-Möller, A. (2015). Exchange of warming deep waters across Fram Strait. *Deep Sea Research Part I: Oceanographic Research Papers*, *103*, 86–100. https://doi.org/10.1016/j.dsr.2015.06.003

Waddell, L. M., & Moore, T. C. (2008). Salinity of the Eocene Arctic Ocean from oxygen isotope analysis of fish bone carbonate. *Paleoceanography*, *23*, PA1S04. https://doi.org/10.1029/2007PA001451

Wei, W., & Lohmann, G. (2012). Simulated Atlantic multidecadal oscillation during the Holocene. *Journal of Climate*, *25*(20), 6989–7002. https://doi.org/10.1175/JCLI-D-11-00667.1

Wright, J. D., & Miller, K. G. (1996). Control of North Atlantic deep water circulation by the Greenland-Scotland Ridge. *Paleoceanography*, *11*(2), 157–170. https://doi.org/10.1029/95PA03696

Zhang, X., Lohmann, G., Knorr, G., & Xu, X. (2013). Different ocean states and transient characteristics in Last Glacial Maximum simulations and implications for deglaciation. *Climate of the Past*, *9*(5), 2319–2333. https://doi.org/10.5194/cp-9-2319-2013